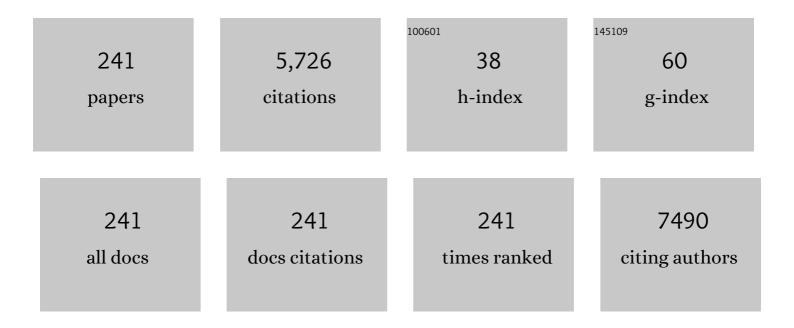
List of Publications by Year in descending order

Source: https://exaly.com/author-pdf/1633565/publications.pdf Version: 2024-02-01



ΙΝCΗΛΙ ΥΛΝΟ

#	Article	IF	CITATIONS
1	A novel strategy for improving SERS activity by cerium ion fÂ→Âd transitions for rapid detection of endocrine disruptor. Chemical Engineering Journal, 2022, 430, 131467.	6.6	8
2	Moisture-preventing MAPbI3 solar cells with high photovoltaic performance via multiple ligand engineering. Nano Research, 2022, 15, 1375-1382.	5.8	29
3	Exploring low-temperature processed multifunctional HEPES-Au NSs-modified SnO2 for efficient planar perovskite solar cells. Chemical Engineering Journal, 2022, 427, 131832.	6.6	12
4	Aptamer-conjugated magnetic Fe3O4@Au core-shell multifunctional nanoprobe: A three-in-one aptasensor for selective capture, sensitive SERS detection and efficient near-infrared light triggered photothermal therapy of Staphylococcus aureus. Sensors and Actuators B: Chemical, 2022, 350, 130879.	4.0	27
5	Photoelectric balance of rear electrode in bifacial perovskite solar cells: Construction of 0D/1D/2D composite electrode based on silver nanowires to boost photovoltaic output. Journal of Power Sources, 2022, 520, 230815.	4.0	7
6	Hydrogen Tetrachloroaurate-Modulated PEDOT:PSS film assembled with conductive NPB buffer layer for High-Performance planar perovskite solar cells. Chemical Engineering Journal, 2022, 432, 134358.	6.6	5
7	Hydrophobic PbS QDs layer decorated ZnO electron transport layer to boost photovoltaic performance of perovskite solar cells. Chemical Engineering Journal, 2022, 439, 135701.	6.6	21
8	Interface synthesis of MoS2@ZnO@Ag SERS substrate for the ultrasensitive determination of bilirubin. Applied Surface Science, 2022, 598, 153750.	3.1	11
9	Enhanced photovoltaic output of bifacial perovskite solar cells <i>via</i> tailoring photoelectric balance in rear window layers with 1T-WS ₂ nanosheet engineering. Materials Chemistry Frontiers, 2022, 6, 2061-2071.	3.2	8
10	Particle Swarm Predictions of a SrB ₈ Monolayer with 12-Fold Metal Coordination. Journal of the American Chemical Society, 2022, 144, 11120-11128.	6.6	12
11	Reinforcing perovskite framework via aminotrifluorotoluene for achieving efficient and moisture-resistance solar cells. Chemical Engineering Journal, 2022, 450, 137990.	6.6	13
12	Enhanced semiconductor charge-transfer resonance: Unprecedented oxygen bidirectional strategy. Sensors and Actuators B: Chemical, 2021, 327, 128903.	4.0	19
13	One-step fabrication of Fe3O4–Cu nanocomposites: High-efficiency and low-cost catalysts for reduction of 4-nitrophenol. Materials Chemistry and Physics, 2021, 260, 124144.	2.0	20
14	A synchronous defect passivation strategy for constructing high-performance and stable planar perovskite solar cells. Chemical Engineering Journal, 2021, 413, 127387.	6.6	40
15	Interface Dipole Induced Fieldâ€Effect Passivation for Achieving 21.7% Efficiency and Stable Perovskite Solar Cells. Advanced Functional Materials, 2021, 31, 2008052.	7.8	40
16	The influence of ZnO loading amount on the photocatalytic performance of Fe ₃ O ₄ @SiO ₂ @ZnO–Ag composites toward the degradation of organic pollutants and hydrogen evolution. New Journal of Chemistry, 2021, 45, 19283-19293.	1.4	2
17	Preferred Film Orientation to Achieve Stable and Efficient Sn–Pb Binary Perovskite Solar Cells. ACS Applied Materials & Interfaces, 2021, 13, 10822-10836.	4.0	16
18	Self-sustainable and recyclable ternary Au@Cu2O–Ag nanocomposites: application in ultrasensitive SERS detection and highly efficient photocatalysis of organic dyes under visible light. Microsystems and Nanoengineering, 2021, 7, 23.	3.4	72

#	Article	IF	CITATIONS
19	Diluted-CdS Quantum Dot-Assisted SnO ₂ Electron Transport Layer with Excellent Conductivity and Suitable Band Alignment for High-Performance Planar Perovskite Solar Cells. ACS Applied Materials & Interfaces, 2021, 13, 16326-16335.	4.0	27
20	In-situ surface-enhanced Raman scattering based on MTi20 nanoflowers: Monitoring and degradation of contaminants. Journal of Hazardous Materials, 2021, 412, 125209.	6.5	40
21	Molecular Coupling and Selfâ€Assembly Strategy toward WSe ₂ /Carbon Micro–Nano Hierarchical Structure for Elevated Sodiumâ€Ion Storage. Small Methods, 2021, 5, e2100374.	4.6	24
22	Fabrication of ZnO/ZnS/ZnSe nanosheets for enhanced photocatalytic activity under simulated solar light. Journal of Materials Science: Materials in Electronics, 2021, 32, 20082-20092.	1.1	3
23	Interior/Interface Modification of Textured Perovskite for Enhanced Photovoltaic Outputs of Planar Solar Cells by an In Situ Growth Passivation Technology. ACS Applied Materials & Interfaces, 2021, 13, 39689-39700.	4.0	8
24	Raman Scattering Methods for Monitoring the Electric Properties of the Postannealed Bulk Heterojunction. ACS Applied Energy Materials, 2021, 4, 8360-8367.	2.5	1
25	Novel carbon quantum dot modified g-C3N4 nanotubes on carbon cloth for efficient degradation of ciprofloxacin. Applied Surface Science, 2021, 559, 149967.	3.1	31
26	Destroying the symmetric structure to promote phase transition: Improving the SERS performance and catalytic activity of MoS2 nanoflowers. Journal of Alloys and Compounds, 2021, 886, 161268.	2.8	18
27	The unconventionally stoichiometric compounds in the Na–K system at high pressures. Computational Materials Science, 2021, 200, 110818.	1.4	2
28	Full-scale chemical and field-effect passivation: 21.52% efficiency of stable MAPbI3 solar cells via benzenamine modification. Nano Research, 2021, 14, 2783-2789.	5.8	20
29	Visible-light-driven photocatalytic degradation of RhB by carbon-quantum-dot-modified g-C ₃ N ₄ on carbon cloth. CrystEngComm, 2021, 23, 4782-4790.	1.3	10
30	A two-fold interfacial electric-field strategy: boosting the performance of electron transport layer-free perovskite solar cells with low-cost and versatile inorganic acid treatment. Journal of Materials Chemistry C, 2021, 9, 12920-12927.	2.7	12
31	Tailoring the d-band center by borophene subunits in chromic diboride toward the hydrogen evolution reaction. Inorganic Chemistry Frontiers, 2021, 8, 5130-5138.	3.0	5
32	Two-Dimensional TeB Structures with Anisotropic Carrier Mobility and Tunable Bandgap. Molecules, 2021, 26, 6404.	1.7	0
33	Constructing 1D Boron Chains in the Structure of Transition Metal Monoborides for Hydrogen Evolution Reactions. Catalysts, 2021, 11, 1265.	1.6	5
34	Unconventional Stoichiometries of Na–O Compounds at High Pressures. Materials, 2021, 14, 7650.	1.3	0
35	lodine-assisted antisolvent engineering for stable perovskite solar cells with efficiency >21.3 %. Nano Energy, 2020, 67, 104224.	8.2	46
36	Constructing "hillocks―like random-textured absorber for efficient planar perovskite solar cells. Chemical Engineering Journal, 2020, 387, 124091.	6.6	12

#	Article	IF	CITATIONS
37	Construction of a direct Z-scheme ZnS quantum dot (QD)-Fe2O3 QD heterojunction/reduced graphene oxide nanocomposite with enhanced photocatalytic activity. Applied Surface Science, 2020, 506, 144922.	3.1	33
38	Pressure-Engineered Optical and Charge Transport Properties of Mn ²⁺ /Cu ²⁺ Codoped CsPbCl ₃ Perovskite Nanocrystals <i>via</i> Structural Progression. ACS Applied Materials & Interfaces, 2020, 12, 48225-48236.	4.0	22
39	Novel insights into the role of solvent environment in perovskite solar cells prepared by two-step sequential deposition. Journal of Power Sources, 2020, 480, 228862.	4.0	9
40	Constructing m-TiO2/a-WOx hybrid electron transport layer to boost interfacial charge transfer for efficient perovskite solar cells. Chemical Engineering Journal, 2020, 402, 126303.	6.6	28
41	Hot-Carrier Injection Antennas with Hemispherical AgO <i>_x</i> @Ag Architecture for Boosting the Efficiency of Perovskite Solar Cells. ACS Applied Materials & Interfaces, 2020, 12, 41446-41453.	4.0	19
42	Construction of an MZO heterojunction system with improved photocatalytic activity for degradation of organic dyes. CrystEngComm, 2020, 22, 7059-7065.	1.3	13
43	Enhanced Magnetic Properties of Co-Doped BiFeO3 Thin Films via Structural Progression. Nanomaterials, 2020, 10, 1798.	1.9	21
44	Recyclable Magnetic MIP-Based SERS Sensors for Selective, Sensitive, and Reliable Detection of Paclobutrazol Residues in Complex Environments. ACS Sustainable Chemistry and Engineering, 2020, 8, 14549-14556.	3.2	39
45	Ho and Ti Co-Substitution Tailored Structural Phase Transition and Enhanced Magnetic Properties of BiFeO ₃ Thin Films. ACS Omega, 2020, 5, 29292-29299.	1.6	9
46	Damping resonance and refractive index effect on the layer-by-layer sputtering of Ag and Al2O3 on the polystyrene template. Spectrochimica Acta - Part A: Molecular and Biomolecular Spectroscopy, 2020, 238, 118430.	2.0	4
47	Fabrication of magnetically recoverable Fe3O4/CdS/g-C3N4 photocatalysts for effective degradation of ciprofloxacin under visible light. Ceramics International, 2020, 46, 20974-20984.	2.3	39
48	Sandwich-like electron transporting layer to achieve highly efficient perovskite solar cells. Journal of Power Sources, 2020, 453, 227876.	4.0	15
49	Highly efficient and recyclable catalyst: porous Fe ₃ O ₄ –Au magnetic nanocomposites with tailored synthesis. Nanotechnology, 2020, 31, 225701.	1.3	13
50	Monitoring the charge-transfer process in a Nd-doped semiconductor based on photoluminescence and Applications, 2020, 9, 117.	7.7	111
51	Detect, remove and re-use: Sensing and degradation pesticides via 3D tilted ZMRs/Ag arrays. Journal of Hazardous Materials, 2020, 391, 122222.	6.5	50
52	The Electric and Dielectric Properties of SrF2:Tb3+ Nanocrystals Revealed by AC Impedance Spectroscopy. Crystals, 2020, 10, 31.	1.0	0
53	Visible light degradation and separation of RhB by magnetic Fe3O4/ZnO/g-C3N4 nanoparticles. Journal of Materials Science: Materials in Electronics, 2020, 31, 5187-5197.	1.1	11
54	Pressure effect on the ionic transport behavior and dielectric property of YF3. Journal of Alloys and Compounds, 2020, 823, 153866.	2.8	3

#	Article	IF	CITATIONS
55	High pressure X-ray diffraction study of sodium oxide (Na2O): Observations of amorphization and equation of state measurements to 15.9ÂGPa. Journal of Alloys and Compounds, 2020, 823, 153793.	2.8	10
56	Carrier dynamic monitoring of a ï€-conjugated polymer: a surface-enhanced Raman scattering method. Chemical Communications, 2020, 56, 2779-2782.	2.2	16
57	Charge Carrier Transport Behavior and Dielectric Properties of BaF2:Tb3+ Nanocrystals. Nanomaterials, 2020, 10, 155.	1.9	0
58	Self-cleaning semiconductor heterojunction substrate: ultrasensitive detection and photocatalytic degradation of organic pollutants for environmental remediation. Microsystems and Nanoengineering, 2020, 6, 111.	3.4	20
59	Tuning the defects and luminescence of ZnO:(Er, Sm) nanoflakes for application in organic wastewater treatment. Journal of Materials Science: Materials in Electronics, 2019, 30, 15869-15879.	1.1	6
60	Unravelling the mechanism of interface passivation engineering for achieving high-efficient ZnO-based planar perovskite solar cells. Journal of Power Sources, 2019, 438, 226957.	4.0	23
61	Fundamental Formation of Three-Dimensional Fe ₃ O ₄ Microcrystals and Practical Application in Anchoring Au as Recoverable Catalyst for Effective Reduction of 4-Nitrophenol. Industrial & Engineering Chemistry Research, 2019, 58, 15151-15161.	1.8	31
62	Detection of DNA Hybridization Using ZnS:Mn2+ Nanowires/SiO2 Core/Shell Nanocomposites and Au Nanoparticles. Journal of Applied Spectroscopy, 2019, 86, 416-421.	0.3	1
63	ZnO nanoparticles on MoS2 microflowers for ultrasensitive SERS detection of bisphenol A. Mikrochimica Acta, 2019, 186, 593.	2.5	47
64	ZnO nanorod arrays decorated with AgCl nanoparticles as highly efficient visible-light-driven photocatalyst. Journal of Materials Science: Materials in Electronics, 2019, 30, 13690-13697.	1.1	5
65	Modulation of Ni3+ and crystallization of dopant-free NiOx hole transporting layer for efficient p-i-n perovskite solar cells. Electrochimica Acta, 2019, 319, 41-48.	2.6	22
66	Engineering 3D hybrid electrode composed of ceria nanoparticles embedded in nickel oxides for high-performance supercapacitors. Journal of Applied Physics, 2019, 126, 015103.	1.1	12
67	Eco-friendly nanostructured Zn–Al layered double hydroxide photocatalysts with enhanced photocatalytic activity. CrystEngComm, 2019, 21, 4607-4619.	1.3	42
68	Plasmon-coupled Charge Transfer in FSZA Core-shell Microspheres with High SERS Activity and Pesticide Detection. Scientific Reports, 2019, 9, 13876.	1.6	11
69	Neodymium doped zinc oxide for ultersensitive SERS substrate. Journal of Materials Science: Materials in Electronics, 2019, 30, 20537-20543.	1.1	8
70	Effect of CdS shell thickness on the photocatalytic properties of TiO2@CdS core–shell nanorod arrays. Journal of Materials Science: Materials in Electronics, 2019, 30, 17682-17692.	1.1	11
71	InBr3 as a self-defensed redox mediator for Li–O2 batteries: In situ construction of a stable indium-rich composite protective layer on the Li anode. Journal of Power Sources, 2019, 439, 227095.	4.0	19
72	Achieving efficient flexible perovskite solar cells with room-temperature processed tungsten oxide electron transport layer. Journal of Power Sources, 2019, 440, 227157.	4.0	24

#	Article	IF	CITATIONS
73	Site-selective growth of Ag nanoparticles controlled by localized surface plasmon resonance of nanobowl arrays. Nanoscale, 2019, 11, 6576-6583.	2.8	34
74	Decomposition and Recombination of Binary Interalkali Na ₂ K at High Pressures. Journal of Physical Chemistry Letters, 2019, 10, 3006-3012.	2.1	10
75	Engineering the mesoporous TiO2 layer by a facile method to improve the performance of perovskite solar cells. Electrochimica Acta, 2019, 318, 83-90.	2.6	9
76	Improved Charge Transfer and Hot Spots by Doping and Modulating the Semiconductor Structure: A High Sensitivity and Renewability Surface-Enhanced Raman Spectroscopy Substrate. Langmuir, 2019, 35, 8921-8926.	1.6	18
77	AgNPs decorated Mg-doped ZnO heterostructure with dramatic SERS activity for trace detection of food contaminants. Journal of Materials Chemistry C, 2019, 7, 8199-8208.	2.7	40
78	Twoâ€Step Selfâ€Assembly CdS/gâ€C ₃ N ₄ Heterostructure Composites with Higher Photocatalytic Performance Under Visible Light Irradiation. Physica Status Solidi (A) Applications and Materials Science, 2019, 216, 1800978.	0.8	7
79	Toward ultra-thin and omnidirectional perovskite solar cells: Concurrent improvement in conversion efficiency by employing light-trapping and recrystallizing treatment. Nano Energy, 2019, 60, 198-204.	8.2	42
80	Controllable Preparation of SERS-Active Ag-FeS Substrates by a Cosputtering Technique. Molecules, 2019, 24, 551.	1.7	13
81	Performance assessment of Pr1â^'xSrxCo0.8Cu0.2O3â^'δ perovskite oxides as cathode material for solid oxide fuel cells with Ce0.8Sm0.2O1.9 electrolyte. Journal of Materials Science: Materials in Electronics, 2019, 30, 5881-5890.	1.1	2
82	Effect of Ag2S shell thickness on the photocatalytic properties of ZnO/Ag2S core–shell nanorod arrays. Journal of Materials Science, 2019, 54, 1226-1235.	1.7	32
83	Activating Old Materials with New Architecture: Boosting Performance of Perovskite Solar Cells with H ₂ Oâ€Assisted Hierarchical Electron Transporting Layers. Advanced Science, 2019, 6, 1801170.	5.6	35
84	Highâ€Performance Cathode Based on Selfâ€Templated 3D Porous Microcrystalline Carbon with Improved Anion Adsorption and Intercalation. Advanced Functional Materials, 2019, 29, 1806722.	7.8	83
85	Structural, magnetic and impedance spectroscopy properties of Ho3+ modified BiFeO3 multiferroic thin film. Journal of Materials Science: Materials in Electronics, 2019, 30, 2942-2952.	1.1	10
86	Facile Synthesis of Fluorescent Nitrogenâ€Doped Carbon Quantum Dots Using Scindapsus as a Carbon Source. Physica Status Solidi (A) Applications and Materials Science, 2019, 216, 1800404.	0.8	10
87	Charge Transfer in an Ordered Ag/Cu ₂ S/4-MBA System Based on Surface-Enhanced Raman Scattering. Journal of Physical Chemistry C, 2018, 122, 5599-5605.	1.5	40
88	Correlation between structural change and electrical transport properties of Fe-doped chrysotile nanotubes under high pressure. Journal of Physics Condensed Matter, 2018, 30, 144008.	0.7	2
89	Crystal Structures and Electronic Properties of Oxygen-rich Titanium Oxides at High Pressure. Inorganic Chemistry, 2018, 57, 3254-3260.	1.9	19
90	Controlled preparation of superparamagnetic Fe3O4@SiO2@ZnO-Au core-shell photocatalyst with superior activity: RhB degradation and working mechanism. Powder Technology, 2018, 327, 489-499.	2.1	43

#	Article	IF	CITATIONS
91	Design of tunable ultraviolet (UV) absorbance by controlling the Ag Al co-sputtering deposition. Spectrochimica Acta - Part A: Molecular and Biomolecular Spectroscopy, 2018, 197, 37-42.	2.0	11
92	Tuning magnetic properties of BiFeO3 thin films by controlling Mn doping concentration. Ceramics International, 2018, 44, 6054-6061.	2.3	32
93	Eco-friendly seeded Fe ₃ O ₄ -Ag nanocrystals: a new type of highly efficient and low cost catalyst for methylene blue reduction. RSC Advances, 2018, 8, 2209-2218.	1.7	41
94	Optimized design of three-dimensional multi-shell Fe3O4/SiO2/ZnO/ZnSe microspheres with type II heterostructure for photocatalytic applications. Applied Catalysis B: Environmental, 2018, 227, 61-69.	10.8	88
95	Mesoporous TiO ₂ coated ZnFe ₂ O ₄ nanocomposite loading on activated fly ash cenosphere for visible light photocatalysis. RSC Advances, 2018, 8, 1398-1406.	1.7	17
96	SERS polarization-dependent effects for an ordered 3D plasmonic tilted silver nanorod array. Nanoscale, 2018, 10, 8106-8114.	2.8	44
97	General strategy for embedding high quality Fe3O4 quantum dots and ZnS:Mn2+ quantum dots in a silica matrix. Journal of Materials Science: Materials in Electronics, 2018, 29, 876-880.	1.1	2
98	Surface agglomeration is beneficial for release of magnetic property via research of rare earth (RE) element-substitution. Applied Surface Science, 2018, 427, 745-752.	3.1	12
99	Structural and electrical properties of InN hollow nanotubes under high pressure. Materials Letters, 2018, 213, 306-310.	1.3	3
100	Effects of Nd concentration on structural and magnetic properties of ZnFe2O4 nanoparticles. Journal of Materials Science: Materials in Electronics, 2018, 29, 3665-3671.	1.1	14
101	Photocatalytic properties of nano-structured carbon nitride: a comparison with bulk graphitic carbon nitride. International Journal of Materials Research, 2018, 109, 129-135.	0.1	5
102	Enhanced catalyst activity by decorating of Au on Ag@Cu2O nanoshell. Applied Surface Science, 2018, 435, 72-78.	3.1	38
103	Ionic Transportation and Dielectric Properties of YF3:Eu3+ Nanocrystals. Nanomaterials, 2018, 8, 995.	1.9	9
104	XPS and Raman study of the active-sites on molybdenum disulfide nanopetals for photocatalytic removal of rhodamine B and doxycycline hydrochlride. RSC Advances, 2018, 8, 36280-36285.	1.7	15
105	Facile Synthesis of Fe3Pt-Ag Nanocomposites for Catalytic Reduction of Methyl Orange. Chemical Research in Chinese Universities, 2018, 34, 871-876.	1.3	13
106	Correlation between Structural Changes and Electrical Transport Properties of Spinel ZnFe ₂ O ₄ Nanoparticles under High Pressure. ACS Applied Materials & Interfaces, 2018, 10, 42856-42864.	4.0	16
107	Enhanced Magnetic Properties of BiFeO3 Thin Films by Doping: Analysis of Structure and Morphology. Nanomaterials, 2018, 8, 711.	1.9	77
108	Realization of 16.9% Efficiency on Nanowires Heterojunction Solar Cells with Dopantâ€Free Contact for Bifacial Polarities. Advanced Functional Materials, 2018, 28, 1805001.	7.8	18

#	Article	IF	CITATIONS
109	Fabrication of P(NIPAAm-co-AAm) coated optical-magnetic quantum dots/silica core-shell nanocomposites for temperature triggered drug release, bioimaging and in vivo tumor inhibition. Journal of Materials Science: Materials in Medicine, 2018, 29, 169.	1.7	12
110	Carrier Density-Dependent Localized Surface Plasmon Resonance and Charge Transfer Observed by Controllable Semiconductor Content. Journal of Physical Chemistry Letters, 2018, 9, 6047-6051.	2.1	36
111	Influence of Mn2+ ions on optical and magnetic property of wurtzite Zn0.98â^'xFe0.01Cu0.01MnxS nanowires. Applied Physics A: Materials Science and Processing, 2018, 124, 1.	1.1	2
112	Tailoring Blue-Green Double Emissions in Carbon Quantum Dots via Co-Doping Engineering by Competition Mechanism between Chlorine-Related States and Conjugated π-Domains. Nanomaterials, 2018, 8, 635.	1.9	16
113	The Study on Degradation and Separation of RhB Under UV Light by Magnetically ZnO/Fe ₂ O ₃ Nanoparticles. Physica Status Solidi (A) Applications and Materials Science, 2018, 215, 1800416.	0.8	9
114	Fe3O4/Au binary nanocrystals: Facile synthesis with diverse structure evolution and highly efficient catalytic reduction with cyclability characteristics in 4-nitrophenol. Powder Technology, 2018, 338, 26-35.	2.1	33
115	Enhanced Catalytic Reduction of 4-Nitrophenol Driven by Fe3O4-Au Magnetic Nanocomposite Interface Engineering: From Facile Preparation to Recyclable Application. Nanomaterials, 2018, 8, 353.	1.9	52
116	Effect of Tb-doped Concentration Variation on the Electrical and Dielectric Properties of CaF2 Nanoparticles. Nanomaterials, 2018, 8, 532.	1.9	10
117	Defects driven photoluminescence property of Sm-doped ZnO porous nanosheets via a hydrothermal approach. Journal of Materials Science: Materials in Electronics, 2018, 29, 16534-16542.	1.1	5
118	The Electrical Properties of Tb-Doped CaF2 Nanoparticles under High Pressure. Crystals, 2018, 8, 98.	1.0	8
119	Structural Phase Transition and Compressibility of CaF2 Nanocrystals under High Pressure. Crystals, 2018, 8, 199.	1.0	10
120	Highly Efficient, Low-Cost, and Magnetically Recoverable FePt–Ag Nanocatalysts: Towards Green Reduction of Organic Dyes. Nanomaterials, 2018, 8, 329.	1.9	21
121	Ag Nanotwin-Assisted Grain Growth-Induced by Stress in SiO2/Ag/SiO2 Nanocap Arrays. Nanomaterials, 2018, 8, 436.	1.9	4
122	Synthesis of porous ZnS/ZnSe nanosheets for enhanced visible light photocatalytic activity. Journal of Materials Science: Materials in Electronics, 2018, 29, 11605-11612.	1.1	15
123	Rare-earth doping engineering in nanostructured ZnO: a new type of eco-friendly photocatalyst with enhanced photocatalytic characteristics. Applied Physics A: Materials Science and Processing, 2018, 124, 1.	1.1	15
124	Tuning red emission and photocatalytic properties of highly active ZnO nanosheets by Eu addition. Journal of Luminescence, 2018, 204, 573-580.	1.5	16
125	Blocking the Formation of Zn2+/Dye Complexes in Dye-Sensitized Solar Cells by Inserting CdS Quantum Dots into Sandwich Layer. Russian Journal of Physical Chemistry A, 2018, 92, 1224-1228.	0.1	3
126	Multiphase TiO2 surface coating g-C3N4 formed a sea urchin like structure with interface effects and improved visible-light photocatalytic performance for the degradation of ibuprofen. International Journal of Hydrogen Energy, 2018, 43, 13284-13293.	3.8	20

#	Article	IF	CITATIONS
127	Effect of thickness and microstructure of TiO ₂ shell on photocatalytic performance of magnetic separable Fe ₃ O ₄ /SiO ₂ /mTiO ₂ coreâ€shell composites. Physica Status Solidi (A) Applications and Materials Science, 2017, 214, 1600665.	0.8	14
128	Design of Hybrid Nanostructural Arrays to Manipulate SERS-Active Substrates by Nanosphere Lithography. ACS Applied Materials & Interfaces, 2017, 9, 7710-7716.	4.0	47
129	Mixed conduction in BaF ₂ nanocrystals under high pressure. RSC Advances, 2017, 7, 12098-12102.	1.7	10
130	High pressure impedance spectroscopy of SrF ₂ nanocrystals. High Pressure Research, 2017, 37, 312-318.	0.4	3
131	Effects of amount of benzyl ether and reaction time on the shape and magnetic properties of Fe3O4 nanocrystals. Powder Technology, 2017, 319, 53-59.	2.1	24
132	Insights into the role of the interface defects density and the bandgap of the back surface field for efficient p-type silicon heterojunction solar cells. RSC Advances, 2017, 7, 26776-26782.	1.7	29
133	Rational synthesis and tailored optical and magnetic characteristics of Fe3O4–Au composite nanoparticles. Journal of Materials Science, 2017, 52, 10163-10174.	1.7	40
134	Plasmonic-induced SERS enhancement of shell-dependent Ag@Cu ₂ O core–shell nanoparticles. RSC Advances, 2017, 7, 16553-16560.	1.7	55
135	The study of structural and optical properties of (Eu, La, Sm) codoped ZnO nanoparticles via a chemical route. Materials Chemistry and Physics, 2017, 194, 29-36.	2.0	40
136	Comparative studies of the structural and magnetic properties in Cu, Co codoped ZnO multilayer films sputtered on different substrates. Journal of Materials Science: Materials in Electronics, 2017, 28, 2949-2953.	1.1	4
137	Enhanced Photovoltaic Performance of CdS Quantum Dotâ€Sensitized Solar Cells Using 4â€Tertbutylbenzoic Acid as Selfâ€Assembled Monolayer on ZnO Photoanode. Physica Status Solidi (A) Applications and Materials Science, 2017, 214, 1700458.	0.8	4
138	Effect of Cr doping on the phase structure, surface appearance and magnetic property of BiFeO3 thin films prepared via sol–gel technology. Journal of Materials Science: Materials in Electronics, 2017, 28, 17490-17498.	1.1	24
139	Increasing local field by interfacial coupling in nanobowl arrays. RSC Advances, 2017, 7, 43671-43680.	1.7	10
140	Pressure driven semi-metallic phase transition of Sb2Te3. Materials Letters, 2017, 209, 78-81.	1.3	9
141	Structural, thermal and electrochemical properties of SrCo0.8Fe0.1Ga0.1O3-δ cathode material for intermediate-temperature solid oxide fuel cells. Journal of Alloys and Compounds, 2017, 727, 27-33.	2.8	6
142	Iron layer-dependent surface-enhanced raman scattering of hierarchical nanocap arrays. Applied Surface Science, 2017, 423, 1124-1133.	3.1	15
143	Facile one-step hydrothermal method to fabricate Fe3O4 quantum dots–graphene nanocomposites for extraction of dye from aqueous solution. Journal of Materials Science: Materials in Electronics, 2017, 28, 2267-2271.	1.1	8
144	Controllable Charge Transfer in Ag-TiO2 Composite Structure for SERS Application. Nanomaterials, 2017, 7, 159.	1.9	41

#	Article	IF	CITATIONS
145	Fabrication and optical property of ZnS:Mn2+ Nanowires/SiO2 Core/Shell Nanocomposites. Journal of Materials Science: Materials in Electronics, 2017, 28, 14293-14297.	1.1	1
146	Tunable bandgap and optical properties of (Eu, Sm) codoped ZnO nanoparticles. Journal of Materials Science: Materials in Electronics, 2016, 27, 11034-11040.	1.1	5
147	Effects of the sputtering gas conditions on the structural, optical and magnetic properties of Cu, Co codoped ZnO multilayer films. Journal of Materials Science: Materials in Electronics, 2016, 27, 9191-9195.	1.1	0
148	Synthesis, characterization and photoluminescence property of La-doped ZnO nanoparticles. Applied Physics A: Materials Science and Processing, 2016, 122, 1.	1.1	13
149	Synthesis and comparison of the photocatalytic activities of ZnSe(en)0.5, ZnSe and ZnO nanosheets. Journal of Alloys and Compounds, 2016, 689, 287-295.	2.8	34
150	Effect of post-annealing temperature on structure and optical properties of Zn1â^'x Cd x O thin films synthesized by magnetron sputtering. Applied Physics A: Materials Science and Processing, 2016, 122, 1.	1.1	0
151	Phase transition and corresponding influence on the yellow-orange Mn2+ emission of ZnS:Mn2+ quantum dots. Journal of Materials Science: Materials in Electronics, 2016, 27, 10504-10509.	1.1	4
152	Preparation of magnetic Fe3O4@SiO2@mTiO2–Au spheres with well-designed microstructure and superior photocatalytic activity. Journal of Materials Science, 2016, 51, 9602-9612.	1.7	27
153	Chemical precipitation synthesis and significant enhancement in photocatalytic activity of Ce-doped ZnO nanoparticles. Ceramics International, 2016, 42, 14175-14181.	2.3	77
154	Mercury species induced frequency-shift of molecular orientational transformation based on SERS. Analyst, The, 2016, 141, 4782-4788.	1.7	24
155	Synthesis of urchin-like Fe ₃ O ₄ @SiO ₂ @ZnO/CdS core–shell microspheres for the repeated photocatalytic degradation of rhodamine B under visible light. Catalysis Science and Technology, 2016, 6, 4525-4534.	2.1	70
156	CoS nanorod arrays with different lenghth used in CdS sensitized ZnO solar cells. Journal of Materials Science: Materials in Electronics, 2016, 27, 1457-1462.	1.1	8
157	Synthesis and photoluminescence characterizations of the Er 3+ -doped ZnO nanosheets with irregular porous microstructure. Materials Science in Semiconductor Processing, 2016, 41, 32-37.	1.9	20
158	Synthesis and photocatalytic performance of ZnO hollow spheres and porous nanosheets. Journal of Materials Science: Materials in Electronics, 2016, 27, 203-209.	1.1	13
159	Controllable synthesis, growth mechanism, structure and optical properties of ZnO–SiO2 nanocomposites. Journal of Materials Science: Materials in Electronics, 2016, 27, 14-22.	1.1	5
160	Preparation and photocatalytic properties of magnetically reusable Fe3O4@ZnO core/shell nanoparticles. Physica E: Low-Dimensional Systems and Nanostructures, 2016, 75, 66-71.	1.3	94
161	Nanocap array of Au:Ag composite for surface-enhanced Raman scattering. Spectrochimica Acta - Part A: Molecular and Biomolecular Spectroscopy, 2016, 152, 461-467.	2.0	24
162	Synthesis of ZnO films in different solvents and their photocatalytic activities. Crystal Research and Technology, 2015, 50, 840-845.	0.6	5

#	Article	IF	CITATIONS
163	Synthesis of Fe3O4@SiO2@ZnO–Ag core–shell microspheres for the repeated photocatalytic degradation of rhodamine B under UV irradiation. Journal of Molecular Catalysis A, 2015, 406, 97-105.	4.8	44
164	Facile synthesis of magnetic-fluorescent and water-soluble ZnS:Mn2+(–SH)/Fe3O4(–SH)/SiO2 core/shell/shell nanocomposites with pure dopant emission. Journal of Materials Science: Materials in Electronics, 2015, 26, 9955-9961.	1.1	2
165	Au/Ag bimetal nanogap arrays with tunable morphologies for surface-enhanced Raman scattering. RSC Advances, 2015, 5, 7454-7460.	1.7	18
166	Reduced operating voltage in nanotubeâ€shaped Ge ₂ Sb ₂ Te ₅ unites by nanosphere lithography. Crystal Research and Technology, 2015, 50, 160-163.	0.6	0
167	Facile Synthesis of Pd–ZnO Microhole Composites with Enhanced Photocatalysis and Its Photoluminescence Properties. Catalysis Letters, 2015, 145, 1041-1046.	1.4	4
168	Modification of the emission colour and quantum efficiency for oxazoline- and thiazoline-containing iridium complexes via different N^O ligands. RSC Advances, 2015, 5, 18464-18470.	1.7	11
169	One-step hydrothermal synthesis of shape-controlled ZnS–graphene oxide nanocomposites. Journal of Materials Science: Materials in Electronics, 2015, 26, 646-650.	1.1	8
170	The effect of structural phase transition on the magnetic properties of BiFeO3 thin films. Journal of Materials Science: Materials in Electronics, 2015, 26, 1283-1290.	1.1	3
171	Structure and optical properties of Zn0.99â^'xCdxMn0.01S quantum dots. Journal of Materials Science: Materials in Electronics, 2015, 26, 2205-2209.	1.1	3
172	Role of oxygen vacancies in V-doped ZnO diluted magnetic semiconductors. Journal of Materials Science: Materials in Electronics, 2015, 26, 2466-2470.	1.1	13
173	Study on growth mechanism and optical properties of ZnSe nanoparticles. Journal of Materials Science: Materials in Electronics, 2015, 26, 3206-3214.	1.1	18
174	Fabrication and comparison of the photocatalytic activity of ZnSe microflowers and nanosheets. Journal of Materials Science: Materials in Electronics, 2015, 26, 8484-8488.	1.1	8
175	Band alignment tuned by 3-PPA SAMs interfacial modification to enhance the conversion efficiency of ZnO/ZnS heterostructure quantum dots sensitized solar cells. Journal of Materials Science: Materials in Electronics, 2015, 26, 6986-6996.	1.1	8
176	Novel BaBi0.05Co0.8Nb0.15O3â^'î´ perovskite oxide asÂcathode material for intermediate-temperature solid oxide fuel cells. International Journal of Hydrogen Energy, 2015, 40, 6935-6941.	3.8	12
177	Fabrication of ZnO nanorods/Fe3O4 quantum dots nanocomposites and their solar light photocatalytic performance. Journal of Materials Science: Materials in Electronics, 2015, 26, 7415-7420.	1.1	10
178	Study on the synthesis and excitation-powerdependent photoluminescence spectrum of ZnSe nanoparticles. Applied Physics A: Materials Science and Processing, 2015, 118, 563-568.	1.1	14
179	Insight into the role of Li ₂ S ₂ in Li–S batteries: a first-principles study. Journal of Materials Chemistry A, 2015, 3, 8865-8869.	5.2	68
180	Enhanced visible light photocatalytic activity of alkaline earth metal ions-doped CdSe/rGO photocatalysts synthesized by hydrothermal method. Applied Catalysis B: Environmental, 2015, 172-173, 174-184.	10.8	123

#	Article	IF	CITATIONS
181	The electrical transportation and carrier behavior of ZnSe under high pressure. High Pressure Research, 2015, 35, 117-122.	0.4	3
182	Biocompatible ZnS:Mn2+ quantum dots/SiO2 nanocomposites as fluorescent probe for imaging HeLa cell. Journal of Materials Science: Materials in Medicine, 2015, 26, 236.	1.7	8
183	Effect of surfactant on the morphology of ZnO nanopowders and their application for photodegradation of rhodamine B. Powder Technology, 2015, 286, 269-275.	2.1	44
184	Effects of pressure on the carrier behavior of HgSe. High Pressure Research, 2015, 35, 372-378.	0.4	1
185	Characterization of SrCo0.7Fe0.2Nb0.1O3â^ cathode materials for intermediate-temperature solid oxide fuel cells. Journal of Power Sources, 2015, 273, 244-254.	4.0	24
186	Cu-Doping Effect on Structural, Optical and Magnetic Properties of Ce-Doped ZnO Nanoparticles. Nanoscience and Nanotechnology Letters, 2015, 7, 517-520.	0.4	4
187	Ordered Nanocap Array Composed of SiO ₂ -Isolated Ag Islands as SERS Platform. Langmuir, 2014, 30, 15285-15291.	1.6	38
188	Fabrication and optical properties of ZnS:Mn2+ quantum dots/SiO2 nanocomposites. Journal of Materials Science: Materials in Electronics, 2014, 25, 4512-4516.	1.1	3
189	Microstructure and magnetic properties of L10 CoPt nanoparticles by Ag addition. Journal of Sol-Gel Science and Technology, 2014, 70, 528-533.	1.1	6
190	Structure and optical properties of Cd-substituted ZnO (Zn1â^'x Cd x O) thin films synthesized by the dc reactive magnetron sputtering. Applied Physics A: Materials Science and Processing, 2014, 117, 895-900.	1.1	3
191	Rapid synthesis and photoluminescence properties of Eu-doped ZnO nanoneedles via facile hydrothermal method. Chemical Research in Chinese Universities, 2014, 30, 538-542.	1.3	6
192	Controllable morphology and tunable colors of Mg and Eu ion co-doped ZnO by thermal annealing. CrystEngComm, 2014, 16, 6896-6900.	1.3	12
193	Highly enhanced photocatalytic properties of ZnS nanowires–graphene nanocomposites. RSC Advances, 2014, 4, 30798-30806.	1.7	36
194	ZnSe nanoparticles of different sizes: Optical and photocatalytic properties. Materials Science in Semiconductor Processing, 2014, 27, 865-872.	1.9	24
195	Effects of Cu addition on the structure and magnetic properties of L10-FePt nanoparticles prepared by sol–gel method. Journal of Sol-Gel Science and Technology, 2014, 72, 156-160.	1.1	6
196	Growth mechanism and room temperature ferromagnetism property of the Zn1â^'xCrxS nanobelts. Journal of Materials Science: Materials in Electronics, 2014, 25, 2574-2577.	1.1	0
197	Advanced research into the growth mechanism and optical properties of wurtzite ZnSe quantum dots. Journal of Materials Science: Materials in Electronics, 2014, 25, 3639-3644.	1.1	5
198	One-step synthesis of bird cage-like ZnO and other controlled morphologies: Structural, growth mechanism and photocatalytic properties. Applied Surface Science, 2014, 319, 211-215.	3.1	20

#	ARTICLE	IF	CITATIONS
199	Effects of surface modification and SiO2 thickness on the optical and superparamagnetic properties of the water-soluble ZnS:Mn2+ nanowires/Fe3O4 quantum dots/SiO2 heterostructures. CrystEngComm, 2013, 15, 6971.	1.3	11
200	Enhanced photocatalytic activity of ZnO microflower arrays synthesized by one-step etching approach. Journal of Molecular Catalysis A, 2013, 378, 1-6.	4.8	28
201	A study of structural, ferroelectric, ferromagnetic, dielectric properties of NiFe2O4–BaTiO3 multiferroic composites. Journal of Materials Science: Materials in Electronics, 2013, 24, 1900-1904.	1.1	54
202	Fabrication, optical and magnetic properties of the Fe doped Zn0.99Mn0.01S nanowires. Journal of Materials Science: Materials in Electronics, 2013, 24, 1955-1960.	1.1	2
203	Enhancement of magnetization in Er doped BiFeO3 thin Film. Journal of Sol-Gel Science and Technology, 2013, 67, 1-7.	1.1	14
204	Synthesis and characterization of aligned ZnO/MgO core–shell nanorod arrays on ITO substrate. Applied Physics B: Lasers and Optics, 2013, 112, 539-545.	1.1	9
205	Comparison of photocatalytic activity of ZnO rod arrays with various diameter sizes and orientation. Journal of Alloys and Compounds, 2013, 580, 205-210.	2.8	34
206	Effects of annealing temperature on the structure and magnetic properties of the L10-FePt nanoparticles synthesized by the modified sol–gel method. Powder Technology, 2013, 239, 217-222.	2.1	17
207	Size-controlled fabrication of ZnO micro/nanorod arrays and their photocatalytic performance. Materials Chemistry and Physics, 2013, 141, 929-935.	2.0	20
208	Effect of annealing temperature on the energy transfer in Eu-doped ZnO nanoparticles by chemical precipitation method. Journal of Materials Science: Materials in Electronics, 2013, 24, 4542-4548.	1.1	15
209	Nanogaps in 2D Agâ€nanocap arrays for surfaceâ€enhanced Raman scattering. Journal of Raman Spectroscopy, 2013, 44, 1666-1670.	1.2	14
210	Influence of annealing temperature on structural, optical and magnetic properties of Zn0.97Cu0.01V0.02O nanoparticles. Journal of Materials Science: Materials in Electronics, 2013, 24, 317-323.	1.1	9
211	Surface effects on the optical and photocatalytic properties of graphene-like ZnO:Eu3+nanosheets. Journal of Applied Physics, 2013, 113, 033514.	1.1	23
212	Synthesis and characterization of nitrogen-doped carbon nanotubes by pyrolysis of melamine. Applied Physics A: Materials Science and Processing, 2013, 113, 735-739.	1.1	14
213	Tailoring the perpendicular exchange bias in [Pt/Co/CoO]n multilayer by tensile stress on curved substrate. Journal of Applied Physics, 2013, 113, .	1.1	7
214	Effects of SiO2 content on the structure and magnetic properties of L10-FePt nanoparticles synthesized by the sol–gel method. Materials Letters, 2013, 91, 348-351.	1.3	10
215	Effects of (P, N) dual acceptor doping on band gap and <i>p</i> -type conduction behavior of ZnO films. Journal of Applied Physics, 2013, 113, .	1.1	32
216	Perpendicular exchange bias of [Pt/Co]n/CoO multilayer on ordered nanosphere arrays. Journal of Applied Physics, 2012, 111, .	1.1	10

#	Article	IF	CITATIONS
217	Zinc oxide nanotubes decorated with silver nanoparticles as an ultrasensitive substrate for surface-enhanced Raman scattering. Mikrochimica Acta, 2012, 179, 315-321.	2.5	25
218	Effect of tube depth on the photovoltaic performance of CdS quantum dots sensitized ZnO nanotubes solar cells. Journal of Alloys and Compounds, 2012, 543, 58-64.	2.8	15
219	Exchange bias of Co/CoO multilayers deposited on nanosphere array. Applied Physics A: Materials Science and Processing, 2012, 108, 363-368.	1.1	8
220	Defects-Mediated Energy Transfer in Red-Light-Emitting Eu-Doped ZnO Nanowire Arrays. Journal of Physical Chemistry C, 2011, 115, 22729-22735.	1.5	143
221	Tunable deep-level emission in ZnO nanoparticles via yttrium doping. Journal of Alloys and Compounds, 2011, 509, 3606-3612.	2.8	74
222	Effects of mineralizing agent on the morphologies and photoluminescence properties of Eu3+-doped ZnO nanomaterials. Journal of Alloys and Compounds, 2011, 509, 10025-10031.	2.8	27
223	Synthesis and optical properties of Eu-doped ZnO nanosheets by hydrothermal method. Materials Science in Semiconductor Processing, 2011, 14, 247-252.	1.9	76
224	Synthesis and characterization of nitrogen-rich carbon nitride nanobelts by pyrolysis of melamine. Applied Physics A: Materials Science and Processing, 2011, 105, 161-166.	1.1	80
225	Direct synthesis of sp ³ â€hybridized BCN compound by high pressure and temperature. Physica Status Solidi (B): Basic Research, 2011, 248, 1132-1134.	0.7	3
226	The effect of ZnO buffer layer on structural and optical properties of ZnO nanorods. Crystal Research and Technology, 2011, 46, 691-696.	0.6	6
227	Effect of Mn doping on the microstructures and photoluminescence properties of CBD derived ZnO nanorods. Applied Surface Science, 2010, 256, 3365-3368.	3.1	37
228	Correlated d ferromagnetism and photoluminescence in undoped ZnO nanowires. Applied Physics Letters, 2010, 96, .	1.5	226
229	Fabrication and photoluminescence of ZnS:Mn2+ nanowires/ZnO quantum dots/SiO2 heterostructure. Journal of Applied Physics, 2010, 108, 044304.	1.1	14
230	Structural and electrical characteristics of high quality (100) orientated-Zn3N2 thin films grown by radio-frequency magnetron sputtering. Journal of Applied Physics, 2010, 108, .	1.1	37
231	Fabrication and optical properties of Ce-doped ZnO nanorods. Journal of Applied Physics, 2010, 107, .	1.1	89
232	Indirect optical transition due to surface band bending in ZnO nanotubes. Journal of Applied Physics, 2010, 108, 103513.	1.1	27
233	Annealing effects on optical properties of low temperature grown ZnO nanorod arrays. Journal of Applied Physics, 2009, 105, .	1.1	123
234	Ferromagnetism in Cu-doped ZnO nanoparticles at room temperature. Journal of Materials Science: Materials in Electronics, 2009, 20, 628-631.	1.1	57

#	Article	IF	CITATIONS
235	Synthesis and Tribological Properties of WSe2Nanorods. Nanoscale Research Letters, 2008, 3, 481-485.	3.1	24
236	Morphology and photoluminescence properties of ZnO nanostructures fabricated with different given time of Ar. Crystal Research and Technology, 2008, 43, 1041-1045.	0.6	23
237	Synthesis and optical properties of ZnO nanorods. Crystal Research and Technology, 2008, 43, 1314-1317.	0.6	16
238	The structure and luminescence characteristics of LaOBr: Tb3+(Dy3+). Journal of Materials Science, 2005, 40, 3725-3728.	1.7	19
239	Effects of nitrogen incorporation on the properties of GalnNAsâ^GaAs quantum well structures. Journal of Applied Physics, 2005, 97, 073714.	1.1	10
240	Deep-level emissions influenced by O and Zn implantations in ZnO. Applied Physics Letters, 2005, 87, 211912.	1.5	262
241	A photocatalyst prepared by NiCo ₂ O ₄ /CNQD-modified carbon fabric heterojunction enhanced visible-light-driven photocatalytic degradation of methyl orange.	1.3	1